PCCP

PAPER

View Article Online
View Journal | View Issue

Cite this: *Phys. Chem. Chem. Phys.*, 2025, **27**, 23627

Spectroscopic and complementary thermodynamic study of liquid, supercooled, and glassy state of ethylene glycol

Matthew Leonard and Bratoljub H. Milosavljevic *

Raman and IR spectroscopy were employed to uncover coalesced/unresolved peaks in the liquid, glassy, and crystalline phases of ethylene glycol (EG) in a temperature range of +24 to −160 °C. The temperature-resolved O–H stretching mode of supercooled EG exhibited continuous changes throughout the studied temperature range, including below the glass transition temperature (T_g = −121 °C). Conversely, the C–H stretching spectrum showed no significant variation within the same temperature range, indicating a complex synchronous change in the C–H···O and O–H···O bonds. Low-frequency (−200 to +300 cm^{-1}) Raman spectra of glassy and crystalline EG were also reported and compared. The Raman spectrum of the C–C–O bending mode of EG was measured with a high signal-to-noise ratio (SNR > 1000), and the temperature-resolved intensity ratio of the *trans*/*gauche* bands was determined. This ratio decreased linearly down to the glass transition temperature, after which it remained constant. The lack of known polarizabilities for these conformers precludes direct thermodynamic determinations. Previous *ab initio* molecular dynamics simulations indicated room temperature *gauche* to *trans* conformer concentrations of 80% and 20%, respectively. Using this result as a benchmark, for the reaction $G \rightleftarrows T$, the corresponding $\Delta_r G = -RT\ln(K_{eq})$ was calculated to be +3.44 kJ mol^{-1}. Applying the van't Hoff equation in processing our temperature-resolved data yielded the following thermodynamic parameters for the same reaction: $\Delta_r H$ = (+3.06 ± 0.07) kJ mol^{-1}, $\Delta_r S$ = (−1.14 ± 0.31) J mol^{-1} K^{-1}, and $\Delta_r G$ = (+3.40 ± 0.12) kJ mol^{-1}. Another [T]/[G] ratio reported in an experimental NMR study was also used in the thermodynamic calculations; the results obtained were compared to the aforementioned data and discussed.

Received 16th July 2025,
Accepted 18th October 2025

DOI: 10.1039/d5cp02718g

rsc.li/pccp

Introduction

Ethylene glycol (EG) is a hydrogen-bond-forming glass former which has been used in various commercial and industrial applications since the early 20th century. These include its use as a component of antifreeze for engines and plumbing, and in sprays applied to airplane wings to prevent ice formation at high altitudes. EG also has cryobiological applications as an ingredient in the mixtures used to cool biological tissues for cryopreservation, whether for long-term storage or for transportation.[1,2] Some of the industrial applications of EG are related to its relatively high viscosity compared to that of water. This difference in viscosity can be explained by the EG molecule's three-dimensional branching hydrogen bond network, which results in overall lower molecular mobility. Due to it being a small molecule which can form multiple hydrogen bonds at each of its two hydroxyl groups, EG has been and continues to be studied in fundamental research including various experimental techniques and molecular dynamics simulations. The corresponding research results may be useful to better understand the temperature resolved molecular dynamics in larger hydrogen-bond-forming molecules such as polysaccharides and sugars, as well as to provide insights into the supercooled liquids phenomenon. In order to understand EG liquid state properties (hydrogen bonding, structural dynamics, molecular clustering, *etc.*), measurements of the density, viscosity, melting point, heat capacity, enthalpy and entropy of fusion, refractive index, surface tension, speed of sound, and various other properties of pure EG have been performed, and the corresponding data interpretation is extensive.[3–24] More specifically, Thomas *et al.* measured the temperature-resolved kinematic viscosities of EG in the temperature range of +8.1 to +167.6 °C. By taking the derivative of the Arrhenius plot and subsequently plotting this against reciprocal temperature, it was found that EG exhibits Arrhenius behavior only in the low temperature region.[12] Recently, a reference correlation for the experimentally determined dynamic viscosities of EG (in the temperature range 263 to 465 K) was produced in order to resolve the apparent discrepancies in the literature, the consideration of which included 60 references; the uncertainty of the correlation was

Department of Chemistry, The Pennsylvania State University, University Park, PA 16802, USA. E-mail: bhm11@psu.edu

4.9% at the 95% confidence level. The correlation was produced based upon a sum of theoretical contributions to the viscosity, including the contribution to the viscosity due to two-body molecular interactions that occur in dilute gases, a term which accounts for the transport properties of moderately dense gases, a term for the divergence of the viscosity near the critical point, and a residual term that accounts for all other effects to the fluid viscosity at high densities.[15] The measurements of the EG viscosity were expanded to the supercooled (248 K) temperature region in our paper published recently.[16] The EG molecular dynamics has also been extensively investigated by a number of authors. Huot *et al.* performed a thermodynamic study of EG–water mixtures, before which the thermodynamic properties of pure EG were determined and interpreted. These include the molar volume (V_m = 55.92 cm^3 mol^{-1}), the cubic expansion coefficient (α = 6.36 × 10^{-1} K^{-1}), the isothermal compression coefficient (κ_T = 3.72 × 10^{-5} bar^{-1}), and the constant pressure and constant volume heat capacities (c_p = 2.69 J K^{-1} cm^{-3} and c_v = 2.37 J K^{-1} cm^{-3}, respectively). The internal pressure (P_i = 510 J cm^{-3}) and the cohesive energy density (D_{ce} = 1006 J cm^{-3}) were also determined according to the following equations:

$$P_i = \frac{T \times \alpha}{10 \times \kappa_T} \quad (1)$$

$$D_{ce} = \frac{(\Delta H_{vap} - RT)}{V_m} \quad (2)$$

where ΔH_{vap} is the enthalpy of vaporization, R is the gas constant, T is the temperature, and the other terms are as previously defined. The authors compared the aforementioned properties of EG to those of other pure liquids and found that EG is a highly associated solvent, as evidenced by its large value of D_{ce} and small value of α. In addition, the authors found that ethylene glycol appears intermediate between ethanol and water in terms of the extent of hydrogen bonding that the molecules experience in the pure liquid. By finding the difference $D_{ce} - P_i$ for water, EG, and ethanol (2248, 496, and 384 J cm^{-3}, respectively), it was concluded that EG is more closely related to ethanol (which is also a glass former) in terms of the contribution of the hydrogen bonding to the cohesion energy.[17] Gubskaya and Kusalik performed a rigorous analysis of several molecular dynamics models in order to specify the best model for EG. Upon choosing the appropriate model, it was concluded that the EG molecule has a tendency to participate in two weak (possibly bifurcated) hydrogen bonds, in addition to four strong ones.[19] Calorimetric studies of the EG liquid have also been performed. Takeda *et al.* used an adiabatic calorimeter to measure the heat capacities of pure EG and 1,3-propanediol in the temperature range from 13 to 300 K. The pure EG was doped with ∼5 mol% glycerol in order to suppress the crystallization and form the glass; the heat capacity of glycerol was accounted for by assuming the additivity of the heat capacities. The glass transition temperature was determined to be 152 K for the doped sample. From the data obtained, the configurational entropy was calculated as a function of temperature. The authors also reported the enthalpy (ΔH_{fus} = 11.86 kJ mol^{-1}) and entropy (ΔS_{fus} = 45.54 J mol^{-1} K^{-1}) of fusion for pure EG, with a corresponding melting temperature T_m = 260.47 K.[20] Parks and Kelley measured the specific heat capacities of crystalline and liquid EG from 88 to 293 K using a copper calorimeter housed within a dewar, and the corresponding enthalpy and entropy of fusion were determined. The noticeable rise in the heat capacity as EG approached the melting point was attributed to premature melting of the sample due to the presence of impurities. The authors also reported the absolute entropy of pure EG at 298 K; it was determined by using the following equation in the range 0 to 90 K:

$$C_v = f(T^n/\theta^n) \quad (3)$$

where C_v is the constant volume heat capacity, f is a universal function for any substance, T is the temperature, θ is a characteristic constant for each substance, and n is dependent on the given substance. The entropy from 90 K to the melting point (T_m = 260.8 K) and from Tm to 298 K was obtained by graphical integration. A comparison of the entropies of methanol, ethylene glycol, and glycerol (32.6, 42.9, and 53.2 cal. K^{-1}, respectively) reveals that there is a difference of 10.3 cal. K^{-1} per addition of a CH(OH) group.[21] The optical properties of EG have also been characterized. Sani and Dell'Oro reported the real (η) and imaginary (κ) parts of the refractive index of ethylene glycol in the range 181 to ∼54 000 cm^{-1} (185 to 55 000 nm). The values of κ were found by collecting the transmittance spectra of the sample at different path lengths, from which the extinction coefficients (and subsequently values of κ) were determined. The values of η were found from the κ values by using the Kramers–Kronig relationship. Hence, the relative errors of the values of η = 0.1 to 0.7%, and the relative errors of the κ values = ∼3 to 20% cited appear to be incorrect.[22] The previous temperature-resolved dielectric spectroscopy study from Blochowicz *et al.* found that the α-relaxation peak in the dielectric loss spectrum of EG does not have a secondary relaxation peak, β; the α peak is accompanied on its high frequency side only by the excess wing, which is characteristic of a type A glass former.[24] The authors found that the glass transition temperature (T_g) was equal to 152.0 K, which was determined by interpolating the $\tau_\alpha(T)$ at τ_g = 100 s. The corresponding fragility index was found by evaluating the numerical temperature derivative of the relaxation time data at Tg; its value was m = 50.0. Our recently published low-temperature differential scanning calorimetry study produced the same value of T_g (152 K) but the fragility index determined from our viscosity data[16] is 30% higher than that published in ref. 24; there is no apparent reason for the discrepancy observed. In addition, numerous studies were performed at room temperature using IR and Raman spectroscopy,[25–52] because these experimental techniques can provide valuable information on hydrogen bonding, structural dynamics, and molecular clustering (see SI).

In this work, in order to gain deeper/complementary insight into the supercooled and glassy states of EG, low-temperature-resolved Raman spectroscopy experiments were performed; in particular, the O–H and C–H stretching modes were scrutinized. Because only the *gauche* conformer exists in the

crystalline state while both the *trans* (*T*) and *gauche* (*G*) conformers exist in the liquid state, it was of interest to obtain the thermodynamic parameters of the $G \rightleftarrows T$ reaction. Hence, the Raman spectrum of the C–C–O bending mode of EG was measured with a high signal-to-noise ratio (SNR > 1000) in the wavenumber region 425–575 cm^{-1}, and the temperature-resolved intensity ratio of the *trans*/*gauche* bands was determined, which was in turn used to obtain the corresponding $\Delta_r H$, $\Delta_r S$, and $\Delta_r G$.

Experimental methods

Anhydrous ethylene glycol (99.8%) was purchased from ACROS Organics and used as received. Small EG sample sizes had to be applied in order to avoid regular crystallization; therefore, a Raman microscope had to be used instead of a typical Raman spectrometer. Two Horiba LabRam HR Evolution Raman Vis-NIR spectrometers were used in this work. The LabRam spectrometers include an Olympus BXFM-ILHS optical microscope and IDS uEye 3 MPix video camera/software. A Diode Nd:YAG 532 nm laser source with a laser power of 30 or 35 mW was used. The spectra collected in the low frequency range (−300 to +600 cm^{-1}) had a spectral resolution of ~0.7 cm^{-1}; this was achieved by setting the confocal pinhole aperture to 50 μm. Spectra in the O–H and C–H stretching region were obtained with an aperture size of 100 μm, resulting in a spectral resolution of ~9 cm^{-1}. BragGrate notch filters were used to allow the collection of low frequency (5–10 cm^{-1}) signals. Spectra were collected using a groove density of 1800 gratings mm^{-1}; the spectra collected in the O–H stretching region were obtained using a groove density of 300 gratings mm^{-1}. Calibration of the Raman spectrometers was performed using a silicon standard prior to each Raman experiment. For temperature-resolved measurements, a Linkam Scientific Instruments heating and freezing stage (model HFS600E-PB4—with four gold-tipped tungsten probes and 4 BNC connectors) was used. The relevant specifications are: Temperature range −196 to 600 °C, Heating/cooling rate up to 150 °C min^{-1}, temperature stability < 0.1 °C, Silver heating block for high thermal conductivity, 100-ohm platinum resistor sensor (1/10th Din Class A to 0.1 °C), Gas tight chamber for atmospheric control, Single ultra-thin lid window −0.17 mm. More data can be found at the following website: **https://www.linkam.co.uk/hfs600e-pb4**. The Infrared spectra of water and EG were collected using a Thermo-Scientific Nicolet iS50 FTIR spectrometer equipped with a diamond cell; the spectral resolution was better than 0.5 cm^{-1}.

Results and discussion

The Raman spectra corresponding to the C–H stretching mode may provide deeper insight into the glass formation instead of crystallization phenomenon. Indeed, it was found that there is no significant change in the spectrum of the liquid to that of the glassy state from +25 °C to −150 °C; however, the Raman spectrum of the crystal at −150 °C differs drastically from that of the liquid (Fig. 1). The positions of the C–H stretching bands corresponding to liquid and crystalline EG reported in this work agree within ±5 cm^{-1} to those reported previously.[27] Another study reported the Raman spectra of EG at room temperature as a function of pressure; the solid EG was formed at pressures higher than 5 GPa. It was found that there was a shift of the peaks towards higher wavenumber as the pressure exerted on the sample increased, as well as the appearance of an additional peak in the C–H stretching region. These bands are shifted by ~100 cm^{-1} from the corresponding peaks of crystalline EG in this work. The assignment of the C–H stretching peaks in the Raman spectrum of the pressurized solid were ascribed to the CH_2 stretching mode but no symmetry analysis of the mode was indicated.[32]

The comparison of the Raman spectra of the glassy and the liquid states in Fig. 1 shows only a small change in the peak positions (~10 cm^{-1} at most); the peak narrowing corresponding to the glassy state can be attributed to the weakened vibrational intensities at low temperatures. As it will be explained later in the text, we found that the three-fold decrease in the EG *trans* conformation concentration accompanies the glass formation at −121 °C. Apparently, no such change affects the symmetric/asymmetric C–H stretching intensity ratio to the same extent. However, the corresponding intensity ratio changes dramatically for the crystalline EG (which has been established to exist purely in the *gauche* form). Therefore, the change in the C–H stretching intensity ratio from the liquid to the crystalline state cannot be solely explained by the absence of the *trans* conformer.

The results of recent *ab initio* molecular dynamics simulations have indicated that intermolecular OH···O distances in liquid EG are much shorter than the intramolecular OH···O distances, indicating that (small) agglomerate geometries involving intermolecular OH···O interactions dominate over those that involve only intramolecular interactions. In addition, the average number of hydrogen bonds per EG molecule in the liquid state was found to be 3.8.[25] On the other hand, the crystal structure of EG (including the hydrogen bonding

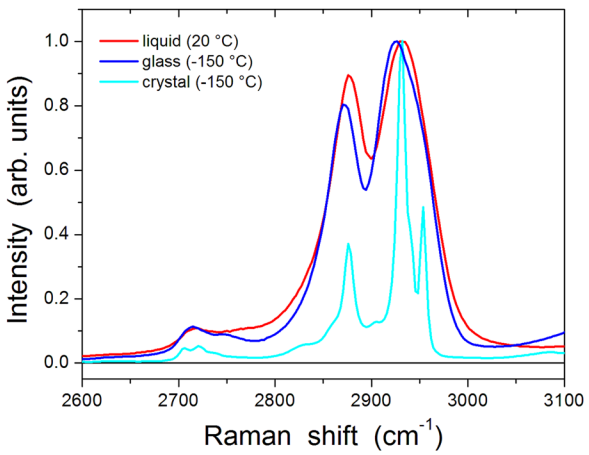

Fig. 1 Raman spectra of the C–H stretching mode of EG in liquid at +20 °C as well as crystalline and glassy state at −150 °C.

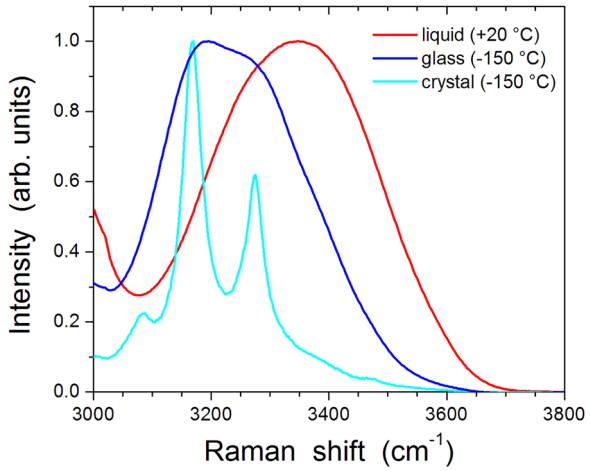

Fig. 2 Raman spectra of the O–H stretching mode of EG in the liquid state at +20 °C as well as the glassy and crystalline state at −150 °C.

between EG molecules) was determined based on a neutron powder diffraction study;[53] it was found that there are 8 total hydrogen bonds in the EG unit cell (4 hydrogen bonds per molecule). Consequently, one possible explanation for the EG glass formation is that the energy of activation for the intramolecular to intermolecular hydrogen bonds conversion is relatively high thus preventing the nucleation center(s) formation.

Fig. 2 presents the Raman spectra in the O–H stretching region for the liquid, crystal, and glassy EG. The spectrum of the crystal agrees with the prior reports.[27,32] There is a clear shift in the O–H stretching mode to lower wavenumbers from the liquid to the glassy phase of EG, however no fine structure was noticeable. In order to make further comments on the O–H stretching mode in EG, the temperature resolved Raman experiment was performed.

Fig. 3 presents the Raman spectra in the O–H stretching region corresponding to the temperature extremes applied in our measurements. The O–H stretching band shifts to lower wavenumbers with temperature and changes continuously, even after the sample forms a glass (−121 °C). There is the appearance of a shoulder on the higher wavenumber side of the spectrum as the sample approaches the glass transition temperature. However, the difference spectral analysis of the Raman spectra in the same wavenumber region shows that there is no isosbestic point in the spectrum, indicating a complex synchronous change in the C–H···O and O–H···O bonds.

The low frequency Raman spectra of the crystal and glassy state of EG are presented and compared in Fig. 4. The crystal spectrum includes multiple sharp peaks in the low frequency region, which have previously been ascribed to the external modes of the EG crystal.[32] These external lattice vibrational modes are due to quanta of energy (low-energy phonons) which excite a given lattice mode within the crystalline structure. The intensities and peak widths of these phonon modes are dependent upon the intermolecular interactions in the crystal, the temperature of the system, and the orientation of the crystalline lattice with respect to the incident laser polarization.[54] Raman scattering due to low energy phonons can also occur in molecular glasses, such as the case for amorphous EG. The Boson peak in the EG glass appears at ∼50 cm^{-1}; in comparison to the crystal peaks, the Boson peak of the glass is broad (peak width of ∼100–200 cm^{-1}). The differences between the Raman spectra of the crystal and the glass can be explained by the distribution of low-energy phonons which can excite the EG vibrational modes. Since there are both short- and long-range orders of molecules in the EG crystal, the quanta of energy which result in excitation of the phonon modes are discrete. In the amorphous EG, there is a random spatial distribution of the molecules, thus resulting in a distribution of vibrational states. Consequently, the corresponding Raman scattering spectra have no fine structure.

The conformational analysis of ethylene glycol has been the focus of numerous studies for several decades. Namely, there has been an interest in establishing the room temperature equilibrium concentrations of the *trans* and *gauche* conformers of EG in the liquid phase. More specifically, there are two equilibria in this system:

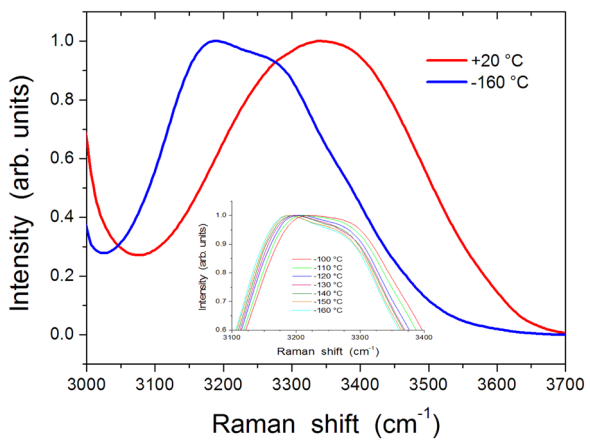

Fig. 3 Raman spectra of the O–H stretching mode in the liquid and glassy state of EG. Insert shows the temperature-resolved Raman spectra near the glass transition temperature (−121 °C).

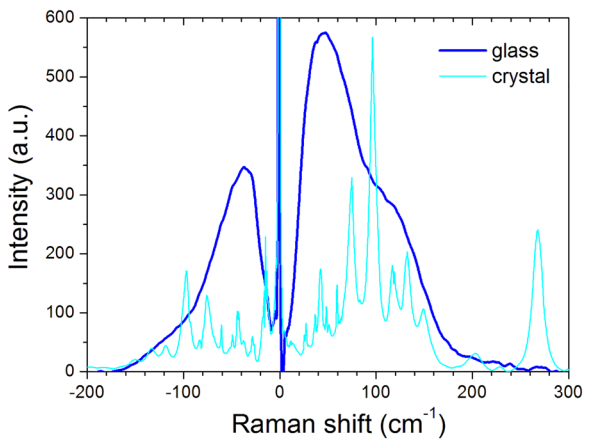

Fig. 4 The low frequency Raman spectra of glassy and crystalline EG at −160 °C. The peak in the crystalline spectrum at −14 cm^{-1} is an artifact of the instrument.

$$G_+ \rightleftarrows T \quad (4)$$

$$G_- \rightleftarrows T \quad (5)$$

where G_+ and G_- are the '*gauche*+' and '*gauche*−' states of EG, respectively. Recently, ref. 28 and 43 reported the *gauche* concentration to be ∼80% at room temperature. Their results were obtained *via* molecular dynamics simulations with improved molecular models and greater computational power than what was previously achievable. If the concentration of the *trans* conformer is 20%, then the concentrations of the *G* enantiomers are 40% each, which adds to 100%. It is pertinent to note that the equilibria (4) and (5) are identical from the kinetic and thermodynamic point of view; therefore, when calculating the equilibrium constant, they can be combined in the following way: $(G_+ + G_-) \rightleftarrows T$, *i.e.*:

$$G \rightleftarrows T \quad (6)$$

where *G* is the *gauche* and *T* is the *trans* conformer of EG. Consequently,

$$K_{eq} = [T]/([G_+] + [G_-]) = [T]/[G] \quad (7)$$

Using the conformer concentrations of 20% *trans* and 80% *gauche* as a benchmark,[28,43] the corresponding $\Delta_r G$ can be calculated using:

$$\Delta_r G = -RT\ln(K_{eq}) \quad (8)$$

with K_{eq} = 20%/80% = 0.25; the corresponding calculated result can be found in the second column of Table 1.

At equilibrium the corresponding reactivities must satisfy the following relation:

$$[G] \times k_{G\to T} = [T] \times k_{T\to G} \quad (9)$$

Apparently, the equilibrium constant for the process described by eqn (6) can be calculated from both the concentration and rate constant ratios:

$$K_{eq} = [T]/[G] = k_{G\to T}/k_{T\to G} \quad (10)$$

In addition to the data obtained from the molecular dynamics simulations, it would be useful to consider a set of experimentally determined equilibrium concentrations. An ^{1}HNMR study reported the concentrations of [G] and [T] in the room temperature liquid to be 86% and 14%, respectively.[37] For the sake of comparison, the corresponding $\Delta_r G$ is also presented in Table 1.

It would be of interest to determine the temperature resolved [T]/[G] ratio, as these data would enable the application of the van't Hoff equation to determine the values of $\Delta_r G$, $\Delta_r H$, and $\Delta_r S$, which may be useful for understanding the EG thermodynamic behavior in the supercooled region. Since our thermodynamic analysis of the temperature-resolved EG conformers' transformations relies on the accuracy of the EG's Raman spectra and the corresponding assignments of its spectral peaks, we measured the room temperature IR and Raman spectra of EG and compared our results to the previously published values, which is presented in Fig. S1 and S5 as well as in Tables S1 and S2 and is accompanied by the relevant discussion. In addition, the Raman spectra of the EG's supercooled and glassy state were compared to the one corresponding to the EG's crystalline state. Only the spectra/modes relevant to the thermodynamic analysis are shown in this section; these are the C–O stretching, C–C–O bending, C–H stretching, O–H stretching and the Boson peak. The entire spectra ranging from −200 to 3800 cm^{-1} (Anti-Stokes and Stokes) are presented/discussed in the SI. Fig. 5 shows the high-resolution Raman spectra corresponding to the C–O

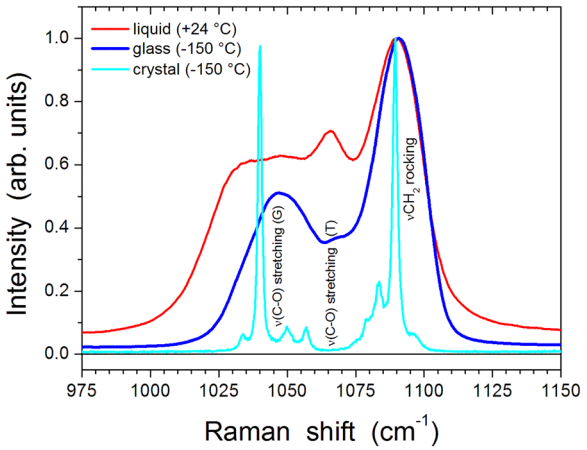

Fig. 5 Raman spectra (resolution = 0.7 cm^{-1}) normalized with respect to the CH_2 rocking mode corresponding to the liquid, crystalline and glassy state of EG.

Table 1 Thermodynamic parameters corresponding to the $G \rightleftarrows T$ conformer reaction, calculated from the room temperature [T]/[G] data[28,37] and our temperature resolved [T]/[G] measurements

	$\Delta_r G = -RT \times \ln(K_{eq})$	$\ln(K_{eq}) = -\frac{\Delta_r H}{RT} + \frac{\Delta_r S}{R}$		
K_{eq}	T = 298 K (kJ mol^{-1})	$\Delta_r H$ (kJ mol^{-1})	$\Delta_r S$ (J mol^{-1} K^{-1})	$\Delta_r G$ (kJ mol^{-1})
20/80	+3.44	+3.06 ± 0.07	−1.14 ± 0.31	+3.40 ± 0.12
14/86	+4.50	+3.06 ± 0.07	−4.71 ± 0.31	+4.46 ± 0.12

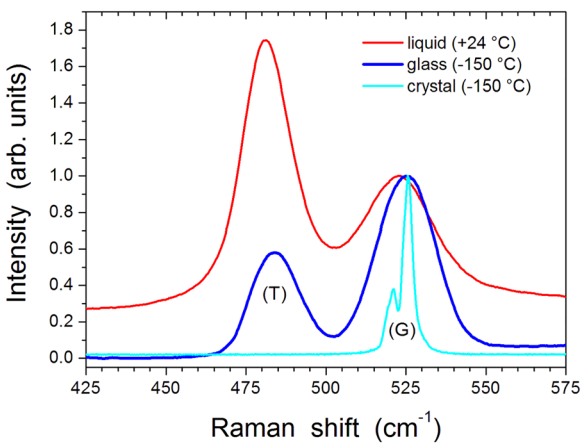

Fig. 6 Raman spectra (resolution = 0.7 cm^{-1}) normalized with respect to the *gauche* conformation of the C–C–O bending mode of EG in the liquid, crystalline and glassy state.

stretching mode of the liquid, crystalline and glassy states of EG. In agreement with previous reports,[27,32] one can see that there is no *trans* conformation (ν = 1062 cm^{-1}) of EG in its crystalline state. However, in the EG glassy state at −150 °C, the *trans* conformation still exists but its concentration is about 50% lower in comparison to that in the liquid state at room temperature. Due to the overlap with the CH_2 rocking peak, the C–O stretching mode is not convenient for the quantitative temperature resolved study of the *trans* to *gauche* conformations' concentration ratio.

Fig. 6 compares high-resolution (0.7 cm^{-1}) normalized Raman spectra corresponding to the C–C–O bending mode of EG in the liquid, crystalline and glassy state. In agreement with previous reports,[27,32] one can see that there is no *trans* conformation (ν = 481 cm^{-1}) of EG in its crystalline state while the *gauche* band is split into two peaks; however, in the EG glassy state at −150 °C the *trans* conformation still exists. Since there is no overlap with other bands, it would be convenient to use the C–C–O bending spectrum to study the temperature-resolved *trans* to *gauche* conformation concentrations' equilibrium.

Fig. 7 shows the temperature-resolved normalized Raman spectra of supercooled liquid and glassy EG in the wavenumber range that corresponds to the C–C–O bending mode. By integrating the *trans* (*T*) and *gauche* (*G*) peaks, the corresponding temperature resolved *T*/*G* intensity ratios were obtained and are shown in the insert of Fig. 7.

In order to obtain the temperature resolved concentration ratios of the conformers from the Raman intensities, the polarizabilities of the *T* and *G* conformations are needed. Namely, the intensity of bands in the Raman spectrum of a compound depends on the change in polarizability α that occurs during the vibration:

$$I_{\text{Raman}} = \text{K} I_{\text{L}} (\tilde{\nu}_0 - \tilde{\nu}_{\text{i}})^4 \left(\frac{\partial \alpha}{\partial Q}\right)^2 \quad (11)$$

where I_{L} is the power of the laser at the sample, $\tilde{\nu}_0 - \tilde{\nu}_{\text{i}}$ the wavenumber at which the band is measured, and $\frac{\partial \alpha}{\partial Q}$ the change in polarizability with the normal coordinate of the vibration.[55] This parameter is the Raman analogy of absorptivity and is sometimes called the Raman cross section. The constant of proportionality, *K*, is dependent on the optical geometry, collection efficiency, detector sensitivity, and amplification.[55] To the best of our knowledge, the value ($\partial\alpha/\partial Q$) and its dependence on temperature for EG are not known. Hence, the peak intensities and the concentrations of the conformers cannot be directly related. One way of solving this problem is to equate the ratio of the areas under their corresponding peaks shown in Fig. 7 to the previously reported [T]/[G] ratio at room temperature. Since the spectral maxima of the *gauche* and *trans* conformers are separated by only 45 cm^{-1}, it is reasonable to assume that the other parameters (contained in constant *K* in eqn (11)) that affect their Raman spectral intensities are the same in this narrow wavenumber interval. The ratio of the conformers' areas at room temperature is 1.8 and that of their concentrations is 0.25. By dividing the two, one finds that the polarizability derivative of the *trans* conformer at room temperature is about 7 times larger than that of the *gauche* one, which is a significant piece of information.

In general, the subject of temperature-resolved polarizability has been very briefly studied both experimentally and theoretically. To get an idea how it depends on temperature, the Clausius–Mossotti relation was employed to calculate the high frequency single-molecule mean polarizability of EG in the temperature range from −70 to +15 °C; the dielectric constants needed were taken from ref. 34 and our extrapolated measured densities were utilized.[16] Due to difficulties in measuring densities and dielectric constants in supercooled liquids at low temperature, the data presented in Fig. S6 are rare in literature and thus valuable for general understanding of the polarizability *vs.* temperature relationship. Hence, it is worth presenting and discussing them in the SI.

It would be interesting/important to see how the [T]/[G] changes in the supercooled region down to the glass transition temperature of EG. Then, another unknown to figure out is the temperature dependence of polarizability of both the *G* and *T* conformers separately. Since the peak positions of the C–C–O bending modes corresponding to the *trans* and *gauche* conformer are separated by only 45 cm^{-1}, it is reasonable to assume that the parameters which are contained in constant K in eqn (11) change in the same manner on changing temperature. Under the aforementioned assumptions, the equilibrium constant for the $G \rightleftarrows T$ reaction can be determined. Fig. 8 shows the temperature-resolved equilibrium constants when the $K_{\text{eq,25 °C}}$ is 0.25 and 0.16. These $K_{\text{eq,25 °C}}$ correspond to the equilibrium concentrations published in ref. 28 and 37, respectively.

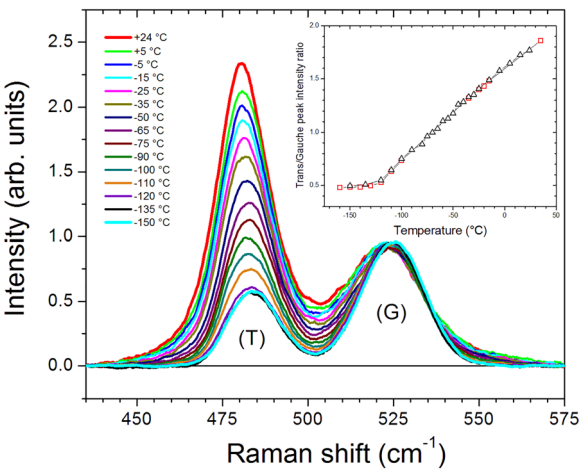

Fig. 7 Temperature-resolved normalized Raman spectra of supercooled liquid and glassy EG in the wavenumber range that corresponds to the C–C–O bending mode; the *trans* and *gauche* conformer bands were labeled as (*T*) and (*G*) respectively. Insert shows the intensity ratios of the (*T*)/(*G*) band areas as a function of temperature. Black triangles and red squares correspond to the 1st and 2nd sets of data, respectively.

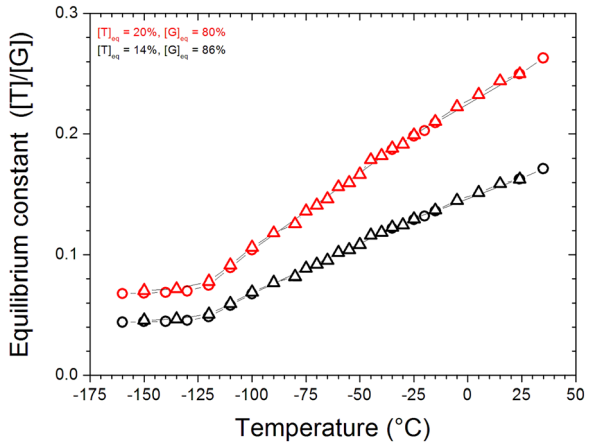

Fig. 8 Temperature-resolved equilibrium constants for the $G \rightleftarrows T$ reaction obtained from the data presented in the insert of Fig. 7 assuming that the $K_{eq,25\,^{\circ}C}$ is 0.25 and 0.16, respectively. Triangles and circles correspond to the 1st and 2nd sets of data from the temperature-resolved Raman experiments, respectively.

For both values of $K_{eq,25\,^{\circ}C}$, the temperature resolved equilibrium constant was found to decrease in approximately linear fashion down to the glass transition temperature (−121 °C), after which it remained constant. Contrary to the crystalline EG, it is apparent from Fig. 8 that the ratio [T]/[G] is not equal to 0 and is a constant value once the sample forms a glass. For the case that $K_{eq,25\,^{\circ}C}$ is equal to 0.25, the concentrations of the conformers below T_g are [T] = 6.5% and [G] = 93.5%. With the temperature resolved equilibrium constant, it is possible to determine the thermodynamic parameters of the conformer reaction using the van't Hoff equation; the corresponding graphs are presented in Fig. 9 and the data obtained are included in Table 1.

The first row of Table 1 corresponds to the equilibrium constant calculated using the estimated concentration of the *trans* conformer [T] = 20% reported in ref. 28, that is, K_{eq} = 0.20/0.80. The second row corresponds to the equilibrium constant calculated using the estimated concentration of the *trans* conformer [T] = 14% reported in ref. 37, that is, K_{eq} = 0.14/0.86. The values of $\Delta_r H$ were found to be equal for the two $K_{eq,25\,^{\circ}C}$ values analyzed, which is not surprising when one realizes that the two trends in Fig. 8 are simply the data in Fig. 7 scaled by two different constants. It is pertinent to note that the van't Hoff plots are linear in the temperature range from +25 to −75 °C indicating the reaction enthalpy is temperature independent in that interval. The positive enthalpy of the reaction $G \rightleftarrows T$ indicates that the intramolecular hydrogen bonds corresponding to the *gauche* conformer in solution are stronger than those corresponding to the *trans* conformer. The value of $\Delta_r S$ is negative for the concentration ratios presented in Fig. 8 (0.25 and 0.16).[28,37] The value of $\Delta_r G$ is positive in both cases. Note that the $\Delta_r G$ calculated from the thermodynamic equilibrium constant is the same as that calculated from the van't Hoff analysis ($\Delta_r G = \Delta_r H - T\Delta_r S$). This can be taken as a piece of evidence that our assumption regarding the conformer polarizabilities (relationship between the Raman intensities and the conformer concentrations) is reasonable. Gaur and Balasubramanian computed (using well-tempered metadynamics simulations using the FF-v1 FF) the free energy difference between the *trans* and *gauche* conformers in the liquid state at room temperature to be 1.7 kJ mol^{-1}.[43] Since there are two *gauche* enantiomers, to get the overall free energy this value should be multiplied by two which gives 3.4 kJ mol^{-1}. This value is in very good agreement with the Gibbs free energy value calculated in our work.

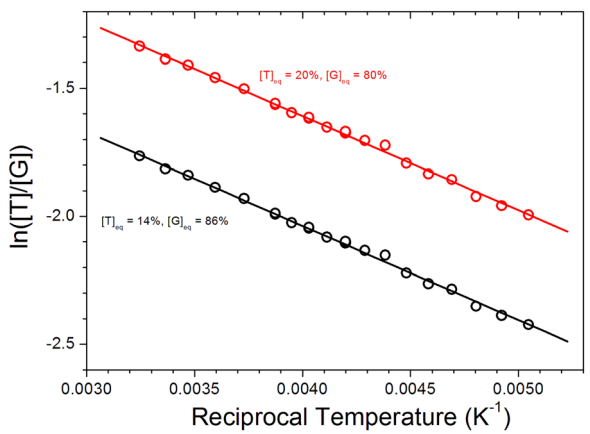

Fig. 9 Van't Hoff plots for the *gauche* to *trans* conformations' reaction obtained from the data presented in Fig. 8. See Table 1 for the corresponding thermodynamic parameters.

Summary and conclusions

Raman and IR spectroscopy were used to reveal coalesced/unresolved peaks and to verify previously published spectra in the liquid, glassy, and crystalline phases of ethylene glycol, EG, in the temperature range from +24 to −160 °C. The precision of our Raman spectral assignments was ±1 cm^{-1}. It was found that the spectral assignments for the room temperature Raman and IR spectra agreed with the literature within ±10 cm^{-1}. The assignments for the Raman spectrum of the crystalline state were found to deviate from the data published previously by as much as 60 cm^{-1}; the C–H and O–H stretching modes deviated by almost 100 cm^{-1}. In addition, five new Raman bands were reported for the crystalline phase; these can likely be attributed to the C–O stretching and the CH_2 scissoring modes. The low frequency (−200 to +300 cm^{-1}) Raman spectra of the glassy and crystalline EG were also reported and compared. The lack of fine structure in the Raman spectra of the glassy EG can be attributed to the random spatial distribution of EG molecules in the glassy state.

We repeated the IR measurement using an anhydrous EG sample and compared the spectrum obtained to that of water. No band was found at 1653 cm^{-1} in the EG spectrum, but a band at 1637 cm^{-1} is observed in the IR spectrum of water, possibly indicating an artefact in ref. 28 due to contamination of EG with water.

The Raman spectrum of the C–C–O bending mode of ethylene glycol was measured in this work with a high signal-to-noise ratio (SNR > 1000), and the corresponding temperature resolved intensity ratio of the *trans*/*gauche* bands was determined. It was found to decrease linearly down to the glass transition temperature (−121 °C), after which it remained constant. The lack of known polarizabilities for these conformers precludes direct thermodynamic determinations. Previously, from *ab initio* molecular dynamics simulations, the room temperature *gauche* to *trans* conformer concentrations were reported to be 80% and 20%, respectively. Using this result as a benchmark, for the reaction $G \rightleftarrows T$, the corresponding $\Delta_r G = -RT\ln(K_{eq})$ was found to be +3.44 kJ mol^{-1}. Using our temperature resolved data, van't Hoff analysis resulted in the following thermodynamic parameters for the same reaction: $\Delta_r H = (+3.06 \pm 0.07)$ kJ mol^{-1}, $\Delta_r S = (-1.14 \pm 0.31)$ J mol^{-1} K^{-1}, and $\Delta_r G = (+3.40 \pm 0.12)$ kJ mol^{-1}. Another [T]/[G] = 0.16 ratio reported in an experimental NMR study was also used in the thermodynamic calculations; the following results were obtained $\Delta_r H = (+3.06 \pm 0.07)$ kJ mol^{-1}, $\Delta_r S = (-4.71 \pm 0.31)$ J mol^{-1} K^{-1}, and $\Delta_r G = (+4.46 \pm 0.12)$ kJ mol^{-1}.

From the analysis of the spectral peak intensities, the polarizability derivative of the *trans* conformer at room temperature was found to be about 7 times larger than that of the *gauche* one.

On cooling, the temperature resolved O–H stretching mode of EG was found to change continuously across a temperature range of +24 to −160 °C, even below the glass transition temperature (−121 °C). On the other hand, we found no significant change in the C–H stretching spectrum in the same temperature range, indicating a complex synchronous change in the C–H···O and O–H···O bonds.

Author contributions

M. L. performed experiments, processed data, and wrote the manuscript. B. H. M. supervised the project and edited the manuscript.

Conflicts of interest

There are no conflicts to declare.

Data availability

The data supporting this article have been included as part of the supplementary information (SI). Supplementary information is available. See DOI: https://doi.org/10.1039/d5cp02718g.

Acknowledgements

We thank the Pennsylvania State University Department of Chemistry for support.

References

1 H. Yue, Y. Zhao, X. Ma and J. Gong, Ethylene glycol: properties, synthesis, and applications, *Chem. Soc. Rev.*, 2012, **41**, 4218–4244, DOI: 10.1039/c2cs15359a.
2 P. Mashouf, N. Tabibzadeh, S. Kuraoka, H. Oishi and R. Morizane, Cryopreservation of human kidney organoids, *Cell. Mol. Life Sci.*, 2024, **81**, 306, DOI: 10.1007/s00018-024-05352-7.
3 A. Ray and G. Nemethy, Densities and Partial Molal Volumes of Water–Ethylene Glycol Mixtures, *J. Chem. Eng. Data*, 1973, **18**, 309–311, DOI: 10.1021/je60058a031.
4 M. Morénas and G. Douhéret, Thermodynamic Behaviour of Some Glycol-Water Mixtures. Excess and Partial volumes, *Thermochim. Acta*, 1978, **25**, 217–224, DOI: 10.1016/0040-6031(78)85009-6.
5 M. Dizechi and E. Marschall, Viscosity of Some Binary and Ternary Liquid Mixtures, *J. Chem. Eng. Data*, 1982, **27**, 358–363, DOI: 10.1021/je00029a039.
6 A. Pal and W. Singh, Speed of Sound and Viscosities in Aqueous Poly(ethylene glycol) Solutions at 303.15 K and 308.15 K, *J. Chem. Eng. Data*, 1997, **42**, 234–237, DOI: 10.1021/je960173x.
7 N. M. Murthy and S. V. Subrahmanyam, Behaviour of excess heat capacity of aqueous nonelectrolytes, *Indian J. Pure Appl. Phys.*, 1977, **15**, 485–489.
8 J. D'Ans, H. Surawski and C. Synowietz, Densities of Binary Aqueous Systems and Heat Capacities of Liquid Systems·CH_2O_2–$C_3H_7NO_2$, *Densities of Liquid Systems*, Landolt-Börnstein Group IV Physical Chemistry 1B. Springer-Verlag, Berlin-Heidelberg, Germany, 1977, DOI: 10.1007/10201852_25.
9 N. G. Tsierkezos and I. E. Molinou, Thermodynamic Properties of Water + Ethylene Glycol at 283.15, 293.15, 303.15, and 313.15 K, *J. Chem. Eng. Data*, 1998, **43**(6), 989–993, DOI: 10.1021/je9800914.
10 T. M. Aminabhavi and B. Gopalakrishna, Density, Viscosity, Refractive Index, and Speed of Sound in Aqueous Mixtures of *N*,*N*-Dimethylformamide, Dimethyl Sulfoxide, *N*,*N*-Dimethylacetamide, Acetonitrile, Ethylene Glycol, Diethylene Glycol, 1,4-Dioxane, Tetrahydrofuran, 2-Methoxyethanol, and 2-Ethoxyethanol at 298.15 K, *J. Chem. Eng. Data*, 1995, **40**, 856–861, DOI: 10.1021/je00020a026.
11 C. Wohlfarth and B. Wohlfarth, *Optical Constants·Refractive Indices of Organic Liquids*, Springer-Verlag, New York, 1996.
12 L. H. Thomas, R. Meatyard, H. Smith and G. H. Davies, Viscosity Behavior of Associated Liquids at Lower Temperatures and Vapor Pressures, *J. Chem. Eng. Data*, 1979, **24**, 161–164, DOI: 10.1021/je60082a011.
13 R. J. Lee and A. S. Teja, Viscosities of Poly(ethylene glycols), *J. Chem. Eng. Data.*, 1990, **35**, 385–387, DOI: 10.1021/je00062a003.
14 C. Yang, P. Ma, F. Jing and D. Tang, Excess Molar Volumes, Viscosities, and Heat Capacities for the Mixtures of Ethylene Glycol + Water from 273.15 K to 353.15 K, *J. Chem. Eng. Data*, 2003, **48**, 836–840, DOI: 10.1021/je020140j.

15 M. Mebelli, D. Velliadou, M. J. Assael and M. L. Huber, Reference correlation for the viscosity of ethane-1,2-diol (ethylene glycol) from the triple point to 465 K and up to 100 MPa, *Int. J. Thermophys.*, 2021, **42**, 116, DOI: 10.1007/s10765-021-02867-0.

16 M. Leonard and B. H. Milosavljevic, Low-temperature study of thermodynamic and rheological properties of ethylene glycol including the supercooled region, *Int. J. Thermophys.*, 2024, **45**, 134, DOI: 10.1007/s10765-024-03426-z.

17 J. Huot, E. Battistel, R. Lumry, G. Villeneuve, J. Lavallee, A. Anusiem and C. Jolicoeur, A comprehensive thermodynamic investigation of water-ethylene glycol mixtures at 5, 25, and 45 °C, *J. Sol. Chem.*, 1988, **17**, 601–636, DOI: 10.1007/BF00645974.

18 H. Matsubara, G. Kikugawa, M. Ishikiriyama, S. Yamashita and T. Ohara, Microscopic picture of heat conduction in liquid ethylene glycol by molecular dynamics simulation: Difference from the monohydric case, *Int. J. Heat Mass Transf.*, 2018, **121**, 1033–1038, DOI: 10.1016/j.ijheatmasstransfer.2018.01.060.

19 A. V. Gubskaya and P. G. Kusalik, Molecular Dynamics Simulation Study of Ethylene Glycol, Ethylenediamine, and 2-Aminoethanol. 1. The Local Structure in Pure Liquids, *J. Phys. Chem. A*, 2004, **108**, 7151–7164, DOI: 10.1021/jp0489222.

20 K. Takeda, O. Yamamuro, I. Tsukushi, T. Matsuo and H. Suga, Calorimetric study of ethylene glycol and 1,3-propanediol: configurational entropy in supercooled polyalcohols, *J. Mol. Struct.*, 1999, **479**, 227–235, DOI: 10.1016/S0022-2860(98)00873-4.

21 G. S. Parks and K. K. Kelley, Thermal Data on Organic Compounds. II. The Heat Capacities of Five Organic Compounds. The Entropies and Free Energies of Some Homologous Series of Aliphatic Compounds, *J. Am. Chem. Soc.*, 1925, **47**, 2089–2097, DOI: 10.1021/ja01685a003.

22 E. Sani and A. Dell'Oro, Optical constants of ethylene glycol over an extremely wide spectral range, *Opt. Mater.*, 2014, **37**, 36–41, DOI: 10.1016/j.optmat.2014.04.035.

23 T. P. Otanicar, P. E. Phelan and J. S. Golden, Optical properties of liquids for direct absorption solar thermal energy systems, *Sol. Energy*, 2009, **83**, 969–977, DOI: 10.1016/j.solener.2008.12.009.

24 T. Blochowicz, C. Gainaru, P. Medick, C. Tschirwitz and E. A. Rössler, The dynamic susceptibility in glass forming molecular liquids: the search for universal relaxation patterns II, *J. Chem. Phys.*, 2006, **124**, 134503, DOI: 10.1063/1.2178316.

25 A. Jindal and S. Vasudevan, Conformation of Ethylene Glycol in the Liquid State: Intra- *versus* Intermolecular Interactions, *J. Phys. Chem. B*, 2017, **121**, 5595–5600, DOI: 10.1021/acs.jpcb.7b02853.

26 A. Jindal and S. Vasudevan, Molecular Conformation and Hydrogen Bond Formation in Liquid Ethylene Glycol, *J. Phys. Chem. B*, 2020, **124**(41), 9136–9143, DOI: 10.1021/acs.jpcb.0c06324.

27 K. Krishnan and R. S. Krishnan, Raman and Infrared Spectra of Ethylene Glycol, *Proc. – Indian Acad. Sci., Sect. A*, 1966, **64**, 111–122, DOI: 10.1007/BF03047675.

28 A. Jindal and S. Vasudevan, Ethylene Glycol Dihedral Angle Dynamics: Relating Molecular Conformation to the Raman Spectrum of the Liquid, *J. Phys. Chem. B*, 2021, **125**(7), 1888–1895, DOI: 10.1021/acs.jpcb.0c10921.

29 A. Jindal, V. Arunachalam and S. Vasudevan, Search for H-Bonded Motifs in Liquid Ethylene Glycol Using a Machine Learning Strategy, *J. Phys. Chem. B*, 2021, **125**(22), 5909–5919, DOI: 10.1021/acs.jpcb.1c01308.

30 R. Ghanghas, A. Jindal and S. Vasudevan, Distinguishing Intra- and Intermolecular Interactions in Liquid 1,2-Ethanediol by ^{1}H NMR and *Ab Initio* Molecular Dynamics, *J. Phys. Chem. B*, 2018, **122**(42), 9757–9762, DOI: 10.1021/acs.jpcb.8b07750.

31 P. Buckley and P. A. Giguère, Infrared studies on rotational isomerism. 1. Ethylene glycol, *Can. J. Chem.*, 1967, **45**, 397–407, DOI: 10.1139/v67-070.

32 C. Murli, N. Lu, Z. Dong and Y. Song, Hydrogen Bonds and Conformations in Ethylene Glycol under Pressure, *J. Phys. Chem. B*, 2012, **116**, 12574–12580, DOI: 10.1021/jp306220q.

33 T. Shimoaka and T. Hasegawa, Molecular structural analysis of hydrated ethylene glycol accounting for the antifreeze effect by using infrared attenuated total reflection spectroscopy, *J. Mol. Liq.*, 2016, **223**, 621–627, DOI: 10.1016/j.molliq.2016.08.097.

34 J. D. Macklis, F. D. Ketterer and E. G. Cravalho, Temperature Dependence of the Microwave Properties of Aqueous Solutions of Ethylene Glycol Between +15 °C and −70 °C, *Cryobiology*, 1979, **16**, 272–286, DOI: 10.1016/0011-2240(79)90039-7.

35 H. Matsuura and T. Miyazawa, Infrared Spectra and Molecular Vibrations of Ethylene Glycol and Deuterated Derivatives, *Bull. Chem. Soc. Jpn.*, 1967, **40**, 85–94, DOI: 10.1246/bcsj.40.85.

36 H. Matsuura, M. Hiraishi and T. Miyazawa, Raman spectra and energy difference between rotational isomers of ethylene glycol, *Spectrochim. Acta, Part A*, 1972, **28**(12), 2299–2304, DOI: 10.1016/0584-8539(72)80209-5.

37 K. G. R. Pachler and P. L. Wessels, Rotational isomerism: X. A nuclear magnetic resonance study of 2-fluoro-ethanol and ethylene glycol, *J. Mol. Struct.*, 1970, **6**(6), 471–478, DOI: 10.1016/0022-2860(70)90029-3.

38 Y. J. Chang and E. W. Castner, Jr., Fast responses from "slowly relaxing" liquids: a comparative study of the femtosecond dynamics of triacetin, ethylene glycol, and water, *J. Chem. Phys.*, 1993, **99**, 7289–7299, DOI: 10.1063/1.465710.

39 M. Schwartz, Raman study of the conformational equilibrium of ethylene glycol in dimethyl sulfoxide, *Spectrochim. Acta, Part A*, 1977, **33**, 1025–1032, DOI: 10.1016/0584-8539(77)80104-9.

40 W. Sawodny, K. Niedenzu and J. W. Dawson, The vibrational spectrum of ethylene glycol, *Spectrochim. Acta, Part A*, 1967, **23**, 799–806, DOI: 10.1016/0584-8539(67)80007-2.

41 P. J. Krueger and H. D. Mettee, Spectroscopic studies of alcohols: Part VII. Intramolecular hydrogen bonds in ethylene glycol and 2-methoxyethanol, *J. Mol. Spectrosc.*, 1965, **18**(2), 131–140, DOI: 10.1016/0022-2852(65)90069-X.

42 A. Gaur and S. Balasubramanian, Conformer Selection Upon Dilution with Water: The Fascinating Case of Liquid Ethylene Glycol Studied via Molecular Dynamics Simulations, *ChemistryOpen*, 2022, **12**, e202200132, DOI: **10.1002/open.202200132**.
43 A. Gaur and S. Balasubramanian, Liquid ethylene glycol: prediction of physical properties, conformer population and interfacial enrichment with a refined non-polarizable force field, *Phys. Chem. Chem. Phys.*, 2022, **24**, 10985–10992, DOI: **10.1039/D2CP00633B**.
44 Y. C. Guo, C. Cai and Y. H. Zhang, Observation of conformational changes in ethylene glycol–water complexes by FTIR–ATR spectroscopy and computational studies, *AIP Adv.*, 2018, **8**, 055308, DOI: **10.1063/1.4995975**.
45 Y. Chen, Y. Ozaki and M. A. Czarnecki, Molecular structure and hydrogen bonding in pure liquid ethylene glycol and ethylene glycol-water mixtures studied using NIR spectroscopy, *Phys. Chem. Chem. Phys.*, 2013, **15**, 18694–18701, DOI: **10.1039/C3CP52146J**.
46 T. Oie, I. A. Topol and S. K. Burt, Ab initio and density functional calculations on ethylene glycol, *J. Phys. Chem.*, 1994, **98**, 1121–1128, DOI: **10.1021/j100055a013**.
47 M. Naganathappa and A. Chaudhari, Mono, di, tri and tetraethylene glycol: Spectroscopic characterization using density functional method and experiment, *Vib. Spectrosc.*, 2018, **95**, 7–15, DOI: **10.1016/j.vibspec.2017.12.006**.
48 R. S. Luo and J. Jonas, Raman scattering study of liquid ethylene glycol confined to nanoporous silica glasses, *J. Raman Spectrosc.*, 2001, **32**, 975–978, DOI: **10.1002/jrs.786**.
49 A. Miyake, CH_2 Rocking Frequencies of Ethylene Glycol and Its Derivatives in Relation to the Configuration of Polyethylene Glycol, *J. Am. Chem. Soc.*, 1960, **82**, 3040–3043, DOI: **10.1021/ja01497a017**.
50 N. A. Chumaevskii, M. N. Rodnikova and J. Barthel, Some peculiarities of compounds with spatial H-bond network: H_2O, H_2O_2, $HOCH_2CH_2OH$, *J. Mol. Liq.*, 2004, **115**, 63–67, DOI: **10.1016/j.molliq.2004.04.001**.
51 E. L. Hommel, J. K. Merle, G. Ma, C. M. Hadad and H. C. Allen, Spectroscopic and Computational Studies of Aqueous Ethylene Glycol Solution Surfaces, *J. Phys. Chem. B*, 2005, **109**(2), 811–818, DOI: **10.1021/jp046715w**.
52 O. B. Zubkova and A. N. Shabadash, A study of the IR spectra of monomeric, dimeric, and trimeric ethylene glycol, *J. Appl. Spectrosc.*, 1971, **14**, 639–643, DOI: **10.1007/BF00605805**.
53 A. D. Fortes and E. Suard, Crystal structures of ethylene glycol and ethylene glycol monohydrate, *J. Chem. Phys.*, 2011, **135**(23), 234501, DOI: **10.1063/1.3668311**.
54 D. Tuschel, Raman Spectroscopy and Imaging of Low Energy Phonons, *Spectroscopy*, 2015, **30**(9), 18–31.
55 Raman spectroscopy, *Volume I, Part 1, Principles and applications in chemistry, physics, materials science, and biology*, ed. G. G. Hoffmann, Momentum Press, New York, 2019.